European Journal of Mechanics B/Fluids 55 (2016) 31–38

Contents lists available at ScienceDirect

European Journal of Mechanics B/Fluids

journal homepage: www.elsevier.com/locate/ejmflu

A novel method to generate tidal-like bores in the laboratory

Germain Rousseaux *, Jean-Marc Mougenot, Ludovic Chatellier, Laurent David, Damien Calluaud

Pprime Institute, UPR 3346, CNRS - Université de Poitiers - ISAE ENSMA, 11 Boulevard Marie et Pierre Curie, Téléport 2, BP 30179, 86962 Futuroscope Cedex, France

ARTICLE INFO

Article history:
Received 12 October 2014
Received in revised form
5 June 2015
Accepted 18 August 2015
Available online 25 September 2015

Keywords:
Tidal bore
Hydraulics
Water waves
Flow visualizations

ABSTRACT

Laboratory experiments are reported where the analogue of a tidal bore is generated with a centimeter-scale local tidal range in a water channel. A discussion of the hydraulic regimes allows to set the experimental conditions to observe the bore. Temporal measurements of the free surface deformation with an acoustic sensor display an analogue of the tidal asymmetry met in nature between the ebb and the flood. Spatial measurements of the free surface deformation are performed with a laser sheet which delineates the interface thanks to the fluorescent re-emission of fluoresceine diluted in water. Afterwards, a parameter space is provided for the observation of a mini-bore with different hydrodynamical regimes (undular, undular–breaking, breaking) by showing the influence of the analogue local tidal range on the shape of the tidal wave. Finally, flow visualizations reveal the inner structure of the velocity profile of the mini-bore in the undular–breaking regime characterized by flow reversals.

© 2015 Elsevier Masson SAS. All rights reserved.

A tidal bore is a tidal phenomenon in which the leading edge of an incoming tide forms a front/wave (or a train of waves) of water that travels up a river or narrow bay against the direction of the river or bay's current [1–7]. Tidal bores are generated by an abnormal local tide that is a tidal wave which has suffered from distortion by non-linearities during its propagation in the estuary. In particular, it has been known since a long time that the quasi-sinusoidal shape of the incoming tide is deformed and becomes non-linear when propagating upstream the river [8–15]. According to historical references like in the following quotation of Brownlie [12], "we discern two abnormal local tidal conditions: (1) the ebb is exceedingly long and slow; (2) the flood is exceedingly short and swift. These conditions are totally different from the usual tidal conditions in the Ocean at the river mouth, therefore they are wholly local; but both are necessary towards the formation of the bore". The shape of the tidal wave is asymmetric between the ebb and flood durations. Nowadays, the terminology "ebb–flood asymmetry" is used to characterize such a behavior. Moreover, the tidal bore often occurs when the wave ascending in a narrowing channel meets in its generation with a bank of sand or elevated bed, which becomes an obstacle to its passage [9–11] since the first waves are caught up by the following waves because of the retardation induced by the obstacle. Here, we report experiments where we create, for the first time, a tidal-like bore with conditions to generate it similar to the ones present in the field namely an ebb–flood asymmetry and the presence of an obstacle at the river entrance albeit without a reduction of the river cross section. We present first the experimental setup and procedures used. Then, we discuss our experimental observations before exploring possibilities for future investigations.

1. The experimental setup

The re-circulating water channel (see Fig. 1) of the Pprime Institute is 6.8 m long. It is characterized by a rectangular cross-section. Its width is $W = 0.39$ m and the water level can be set up to 0.5 m. The flow rate per unit width $q = Q/W$ ranges up to 0.172 m^2/s and is controlled by a PCM Moineau pump featuring an eccentric bearing, an endless screw and a speed controller. It generates a current which passes through a honeycomb and a 3D convergent chamber where the fluid is accelerated by a double constriction in both width and height to suppress vortices at the entrance of the channel and boundary layer effects. The resulting velocity profile at the end of the convergence chamber is almost flat in the vertical direction. Then, the fluid flows along the channel and visualizations are made through the transparent side windows. An exit chamber is located at the very end of the channel where the fluid is re-injected into the pump, and a sluice gate is placed at its entrance in order to control the water depth and flow regimes. In our experiments, the sluice gate is set in the lowest position such

* Corresponding author.
E-mail address: germain.rousseaux@univ-poitiers.fr (G. Rousseaux).

http://dx.doi.org/10.1016/j.euromechflu.2015.08.004
0997-7546/© 2015 Elsevier Masson SAS. All rights reserved.

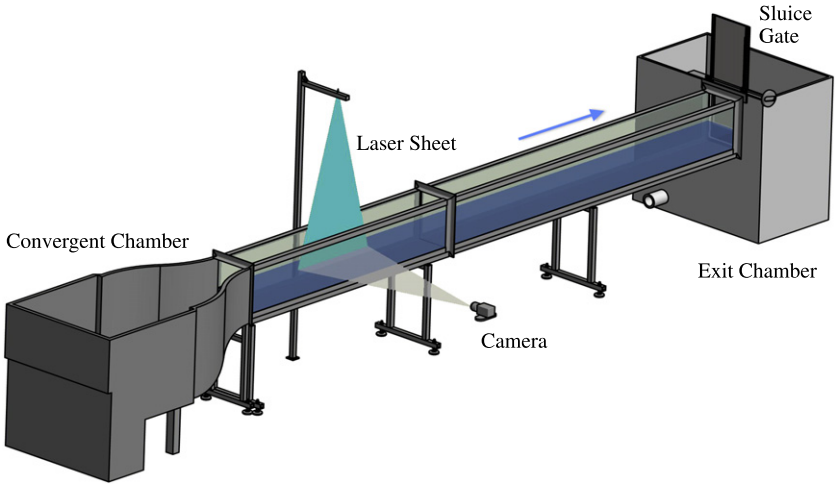

Fig. 1. A sketch of the experimental setup with the laser sheet and the side camera. The arrow indicates the direction of the water current: the bore propagates in the reverse direction.

that the water level is free: depending on the regime, a spillway is generated or not and the water depth adapts itself.

To visualize free surface deformations, an Argon LASER (Spectra Physics $2W$) is used with a light fiber and a cylindrical lens in order to produce a vertical laser sheet with a thickness of 2.5 mm whose trace is located on the middle of the channel width. The laser trace on the flat free surface is centered at 1.5 m from the channel entrance (namely the convergent exit) and extends on 3 m. We diluted 50 g of fluoresceine in the water channel with a static depth of 0.24 m initially. The laser intensity is set such that the sheet only penetrates on a small depth typically of a few mm, thanks to the absorption by the fluorescent dye. A CCD black and white camera (Pulnix RM-4200CL 2048p^2) records the laser trace of the free surface through the channel side window on roughly 1 m along the longitudinal direction of the bore. An additional digital camera (Canon Powershot SX40 HS) is used for colored pictures and movies. In addition, an acoustic sensor (Microsonic mic+24/IU/TC) with a resolution of 0.1 mm measures the water depth at a given place. As its position was varied in the course of experiments, the acoustic sensor is not represented in the setup scheme contrary to the laser sheet which was fixed.

2. The hydraulic regimes and procedures to generate the bore

Concerning the terminology, we will call the static (dynamical) depth h_0 (h_d), the water depth in absence (presence) of a flow. The water depth $h(x, t)$ is both a function of space and time in presence of the bore. By varying the initial static water depth, the sluice gate position and the flow rate of the pump, we can generate different hydraulic regimes with specific flow currents and corresponding dynamical water depths. Since the seminal experiments by George Bidone in 1825 [16] and in order to reproduce a propagating bore in the laboratory [1,17–19], a second sluice gate (not represented in Fig. 1) is placed upstream of the regulation gate and operates as a "guillotine". The gate moves downwards from a initial upper position before being stopped at a given height below the water level. It can be closed partially or completely and then, it blocks the flow. In practice, there is always a small leaking stream below the gate in order that the closing gate does not deteriorate the bottom of the water channel. This closing process creates a sudden rise in the water level and generates a tidal-like body of water which propagates against the flow direction [16,1,17–19]. This procedure is qualified as the "classical" one. In the same vein, sudden changes of the discharge in canals (due to a valve for example) have been studied since the time of Darcy and Bazin and produces similar surges that do not differ from the closing ones [20–23]: they are often described as positive surges from downstream in treatise on hydraulics [24]. Now, a new "natural" procedure mimicking the effect of a tidal wave entering a river is introduced. Of course, it is impossible to reproduce a true tide in the laboratory but it will be shown how to use the hydraulic regimes of the water channel (see the Appendix for details) in order to produce an analogue of the ebb–flood asymmetry encountered in tidal rivers.

The following procedure was chosen to create a laboratory bore with tidal-like conditions. Let us illustrate it with a practical example. First, the static water height is set at $h_0 = 25$ mm; then, the pump is fixed at a given flow rate (for example $q_0 = 0.0215$ m^2/s); the dynamical water depth increases and then stabilizes in a state of equilibrium: one observes a small negative mean slope on the entire channel length due to head losses (mainly because of viscous dissipation); the dynamical water height reaches roughly $h_d = 50$ mm. Now the crucial point: we turn off the pump. The flow rate does not go to zero instantaneously but with a time evolution depending on the pump characteristics and the water channel geometry. It is outside the scope of the paper to understand the precise dynamics of this "closed water system" with the associated equilibrium between the water bodies formed by both chambers and the channel. The dynamical water level in the channel drops rapidly with time as measured with the acoustic sensor (see Fig. 2 (bottom)): it is the analogue of time series of tide elevation.One recovers the typical ebb–flood asymmetry as observed in the field (see the recent survey by Bonneton et al. [4,7] and the often ignored older papers [8–15]) where a long ebb is followed by a short flood at the foot of which the bore is generated. We do believe that this is the main signature of the tidal-like bore formation which makes us believe in the "naturalness" of our laboratory procedure.

The decreasing water depth reaches a minimum (at a given time that we call the time of reversal t_r, here 30 s for $h_0 = 15$ mm in Fig. 2 (bottom)) which is lower than the static and initial water depth h_0 and where the slope suddenly changes its sign. This height at reversal that we denotes h_r is a function (data not reported here) of the static water depth h_0 and one has always $h_r < h_0$: for the case of Fig. 2 (bottom) corresponding to $h_0 = 15$ mm, the minimum water depth is $h_r = 11.5$ mm. The time at reversal t_r increases with the initial flow rate. Then, a sudden rise follows this very long diminution of height. We can explain this behavior by considering that the analogue of the local tidal range in our natural procedure is the parameter $h_0 - h_r$ whereas the global tidal range would be $h_d - h_0$ recalling that h_d is a function of both the initial

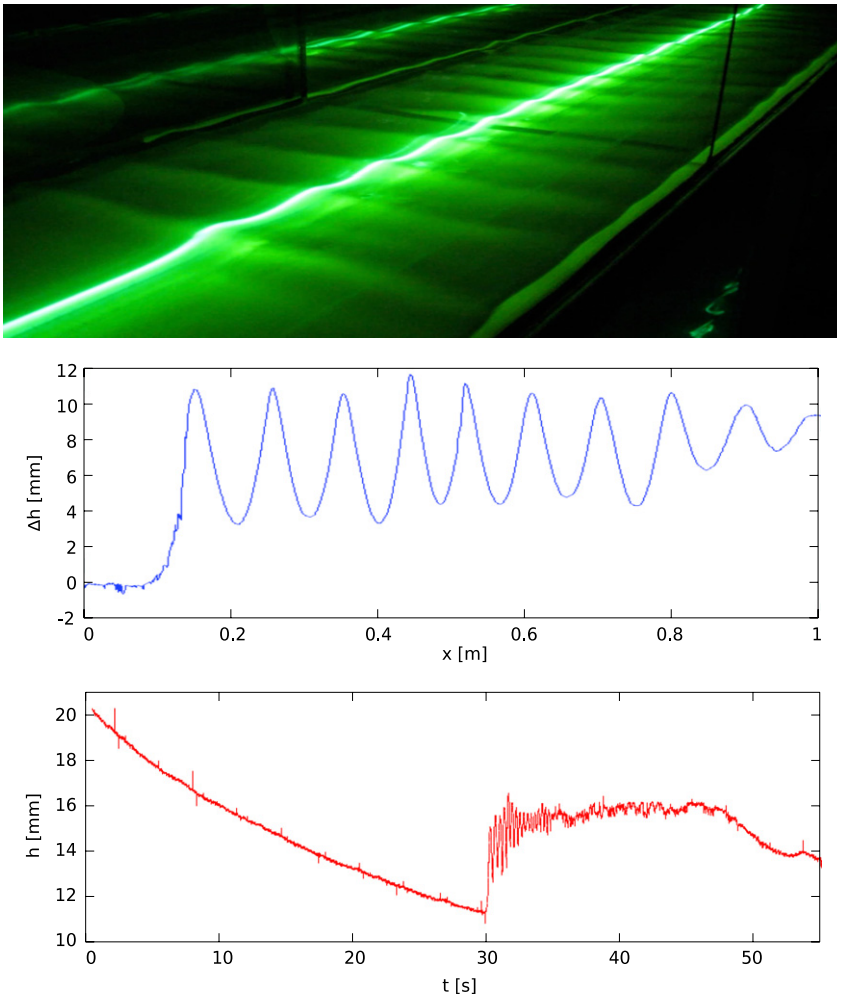

Fig. 2. Top: A mini-bore in the laboratory seen in a perspective with a color camera using a laser sheet and fluorescent dye (the distance between the two vertical black bars corresponds to the channel width $W = 0.39$ m; $h_0 = 25$ mm and $q_0 = 0.0215$ m^2/s). Middle: Surface deformation $\Delta h(x) = h(x) - h_r$ measured with the fluorescence signal as a function space ($h_0 = 25$ mm and $q_0 = 0.0215$ m^2/s). Bottom: Water depth h(t) measured with the acoustic sensor with an ebb–flow asymmetry as a function of time ($h_0 = 15$ mm and $q_0 = 0.0107$ m^2/s); the time at reversal t_r is at 30 s and the height at reversal reaches $h_r = 11.5$ mm.

flow rate q before turning off the pump and h_0. The level difference between the water depths at the end of the measuring section and in the exit chamber is a function of the flow rate. If the latter increases, then the triggering time for the appearance of the bore is longer but it does not change, to the best of our measurements, the bore characteristics. The bore starts to appear precisely when the water levels difference disappears.

After stopping the pump, there is an accumulation of a body of water due to the current deceleration in the exit chamber where the fluid is usually sucked by the pump to be re-injected in the channel inlet. The exit of the channel features a shock or spillway depending on the hydraulic regimes discussed in the Appendix. The shock/spillway plays the role of an entrance obstacle for the oscillations mode of the exit chamber and its effect is similar to the effect of a sand bank in natural river where the tide does accumulate before its strength is suddenly released [9–11]. A mini-bore is emitted spontaneously from the end of the channel back in the opposite direction to the dying current (see Fig. 2 (top)). The role of the exit chamber is tremendous since the water depth is originally higher in the channel before stopping the pump; then, the exit chamber water level increases to the detriment of the channel water level while the shock/spillway disappears; at the end of the process, the chamber level becomes higher than the decreasing river level: a tidal-like range is thus generated. The mean level after the reversal corresponds roughly to h_0.

3. The physical characteristics of the bore

The generated mini-bore is a non-equilibrium system since it appears in the phase where the pump is turned off. However, the measurements are performed a few seconds after stopping the pump and the water level has had the time to decrease tending to the reverse height h_r before recovering the initial water depth h_0 for the mean depth. Moreover, because of inertia, the current is still flowing against the mini-bore as we will demonstrate below. The latter propagates in the channel on a time duration smaller that the time scale needed for the current to vanish or change significantly. Somehow, the flow is in a quasi-static regime even at non-equilibrium where the river current would have been constant and not relaxing. Thanks to the laser line, one observes an undular bore [1] in Fig. 2 (middle) featuring a leading edge followed by so-called stubbles or whelps (secondary oscillations moving at the same speed as the front). The number of stubbles is quite impressive (around thirty). Sometimes, one observes during the propagation along the channel, some coalescence and/or rearrangement of the stubbles (with some similarities with the Eckhaus instability in patterns formation [25]) before reaching a stationary undulation in the moving frame of the bore. Moreover, there are some rearrangement of their parallelism in the few seconds during which the tidal range is transforming into a mini-bore at the very end of the channel. In Fig. 2 (bottom), the high

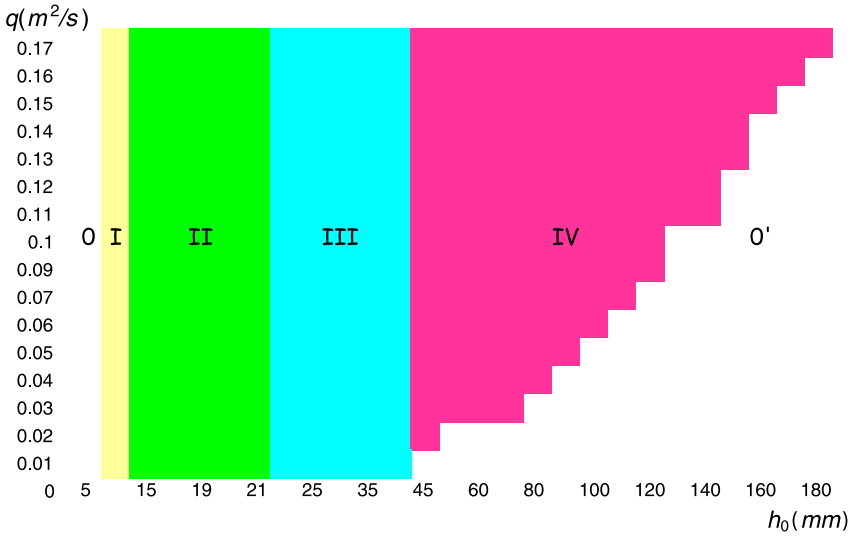

Fig. 3. Phase–space diagram of the mini-bore: the initial flow rate q as a function of the initial and static water depth h_0. 0 and 0': no bore; I: dying bore; II: undular bore; III: undular–breaking bore; IV: breaking bore.

period around 0.5 s corresponds to the stubbles whereas the low frequency (period of 2–3 s between $t = 30$ s and $t = 37$ s) may be associated to either 3D effects or local rearrangements. After $t = 47$ s, the mean water level drops and this is the main difference with the usual increase of the water level after the bore passage due to the incoming tide. The drop in the water level is due to the finite volume of water accumulated in the exit chamber which is able to generate the bore.

4. The phase–space diagram and the role of the analogue tidal-like range

Depending on the initial water depth h_0 and the flow rate q, one can identify by visual means two regimes and six regions of interest in the corresponding parameter space, namely the phase–space diagram (Fig. 3). The two regimes are separated by the initial water depth of 40 mm. For depth inferior to 40 mm, we observed that there is no effect of the initial value of the flow rate on the formation of the mini-bore. A spillway or a shock triangle (as discussed previously) is always generated at the exit of the channel. The bore generation happens when the exit obstacle (be it the spillway or the shock triangle) disappears. A universal relaxation law with time (see Fig. 2 (bottom) before $t = 30$ s) of the dynamical water depth is recovered after a transient, no matter the value of the flow rate (only the duration changes: the higher the flow rate, the longer the relaxation time).

We classified our results by Roman numbers in Fig. 3. 0: no mini-bore is generated or observed by eyes; I: an undular bore is generated but dies during its propagation on the counter-current along the channel; II: an undular bore is generated and propagates on the entire length of the water channel; III: the front and/or subsequent stubbles of the bore are breaking. IV: the bore is breaking and the first stubble disappears in a turbulent body of water moving with the front, then stubbles are sometimes recovered on the tail of the bore. For depths superior to 40 mm, the condition of existence of the bore does depend on the initial flow rate since for small flow rates and high initial water depths, the flow does not go supercritical and no bore is generated in the decelerating phase of the pump: 0′. Thus, there exits a boundary between the region IV and 0′ and an explicit dependence with the flow rate concerning the observation or not of a breaking bore.

Tidal jumps can be present in rivers where visually one would even conclude with the absence of a tidal bore. Indeed, height sensors are able to capture the propagation of the tidal wave. By measuring time series of tide elevation for several local tidal ranges, Bonneton et al. [4,7] have shown the influence of the local tidal range on the front shape of the tidal jump. To simplify, for a small local tidal range, only an elevation in time is measured without an inflection point. For a higher local tidal range, an inflection point is observed which is the signature of a tidal jump even though one does not see a tidal bore visually. Then, a tidal bore is observed as usual for the highest local tidal ranges. We recover such a phenomenology in our experiments, which strengthens our belief in the fact that our procedure is equivalent to what happens in the field. Indeed, by varying the initial water depth h_0 which plays the role of the local tidal range in our experiments (see our discussion above since the height at reversal h_r is function of h_0), we are able to recover the different regimes described by Bonneton et al. in [4,7]. The water depth was measured as a function of time with the acoustic sensor at a given distance of the exit chamber (2.47 m) for different initial water depths h_0: our Fig. 4 is the exact counterpart of Fig. 3 in the work of Bonneton et al. [4].

5. Flow visualizations

To check for the presence of the river counter flow even in our non-equilibrium situation during relaxation of the dynamical water depth, some flow visualizations and velocity measurements using seeded tracers in the fluid were done. In Fig. 5, we report for the streamlines inferred from long time exposure by the CCD camera of the tracers. After stopping the pump, the dynamical water depth decreases on a sufficiently fast time scale for the current to continue to flow; the streamlines are almost parallel with a negligible boundary layer (see Fig. 5(a) where the current is going to the right). Hence, the flow is almost uniform within the channel section and varies only with the longitudinal direction but on a longer time scale which is sufficient for the mini-bore to counter-propagate on the current. Let us underline that the laboratory bore is not similar to a dam break problem on a wet bottom with a given water depth but features one of the necessary ingredient involved in the formation of a tidal bore namely a counter-current and not a static water layer.

When the mini-bore propagates, the parallel streamlines of the river are deviated upwards due to the conflict between the river and the tidal-like wave. Close to the free surface, the deviated jet reversed on an upper layer (see Fig. 5(b)). In addition and for this

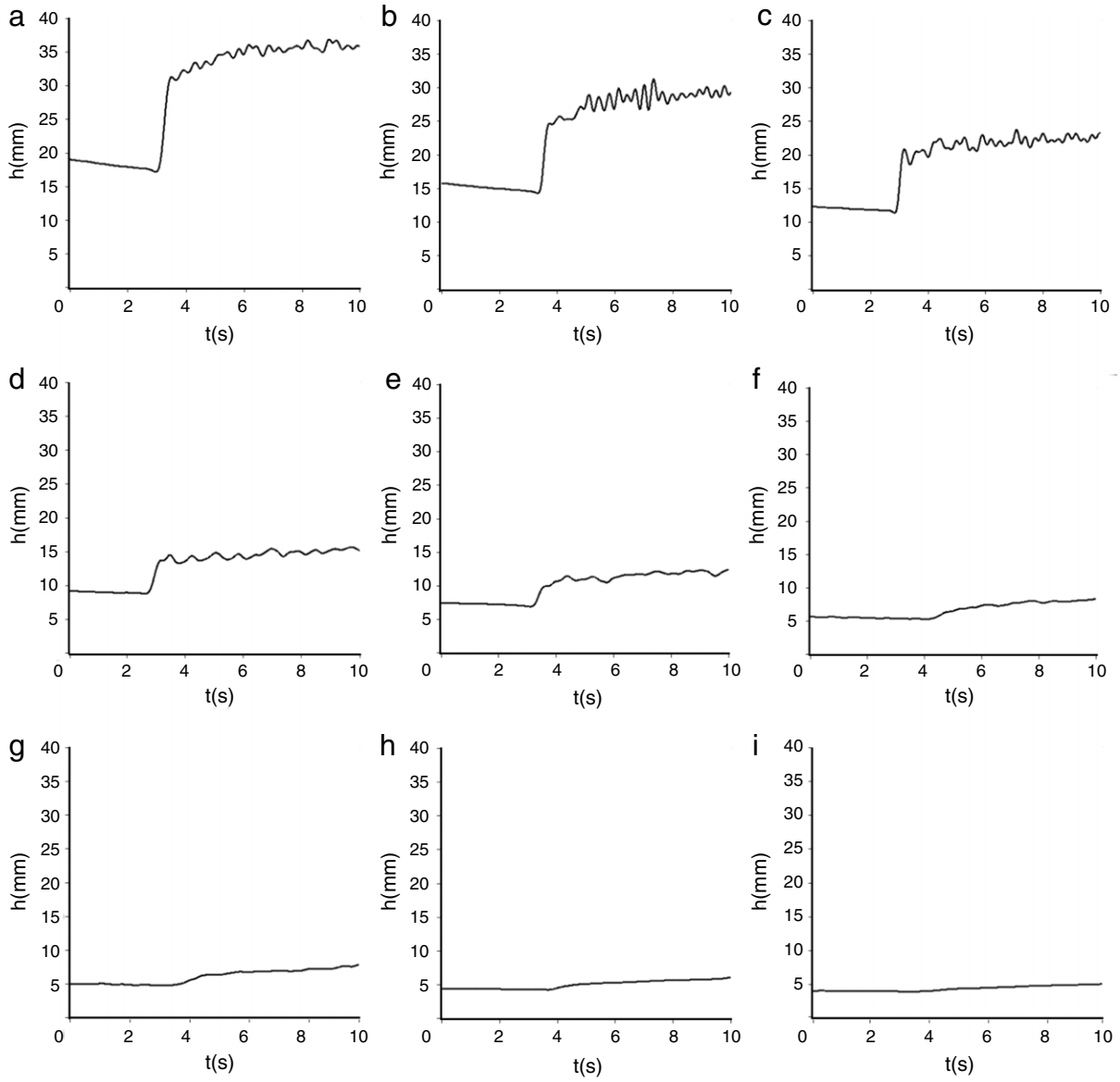

Fig. 4. Influence of the "local tidal range". h_0 = (a) 30 mm, (b) 25 mm, (c) 20 mm, (d) 15 mm, (e) 12.5 mm, (f) 10 mm, (g) 9 mm, (h) 8 mm, (i) 7 mm.

particular $h_0 = 25$ mm, a saddle-point revealing a characteristic "elephant-foot" pattern of streamlines is observed between the leading front and the first whelp, which is an indicator of a boundary layer separation (see the red arrows in Fig. 5(c)). Each stubble is characterized by the usual streamlines pattern for sinusoidal water waves with a portion of concave arches relating the fore and aft fronts (see the blue arrows in Fig. 5(c)). The elephant-foot pattern is reproduced on subsequent stubbles and then vanishes progressively since the stubbles amplitudes decrease. The streamlines patterns of the latter stubbles are similar to a train of deep water waves with decreasing amplitude. A flow reversal is observed at latter times when the mini-bore has almost disappeared. Analysis of Fig. 5(a) allows us to infer an order of magnitude of the velocity field v for the current. Indeed, we measure a typical length for the particles streaks. Given the exposure time, we deduce that the mean velocity of the river current is $v = 0.21$ m/s just before the arrival of the leading front. From the corresponding movie, we track the saddle-point of the "elephant-foot" pattern which moves at the same speed as the leading front to compute the velocity of the mini-bore and the velocity of the bore is found to be $c = 0.49$ m/s. The tidal bore Froude number is computed in the moving frame of the bore (with $h_0 = 25$ mm) $F_r = \frac{v-(-c)}{\sqrt{gh_0}} = \frac{v+c}{\sqrt{gh_0}} = 1.4$. According to the usual classification [1], the laboratory bore we studied for flow visualization is a transitional one between the undular and breaking bores regimes. It is characterized by a small "breaking" in the leading front followed by non-breaking stubbles.

6. Conclusion

A bore created with "natural conditions" like the spontaneous local tidal range generated in the exit chamber of a water channel with its characteristic ebb–flood asymmetry was studied. A parameter space was provided (initial flow rate versus the static water depth) where one distinguishes several kinds of laboratory bore that were identified by visual means coupled to height measurements (undular, undular–breaking, breaking…). The new method for generating a tidal-like bore in the laboratory differs from the usual one featuring a fast-closing gate. We have identified the local tidal range $(h_0 - h_r)/h_r$ as a possible new dimensionless parameters of a geometrical character: in practice, as the height at reversal h_r is a function of the initial height h_0, the local tidal range is only a function of h_0. A future study

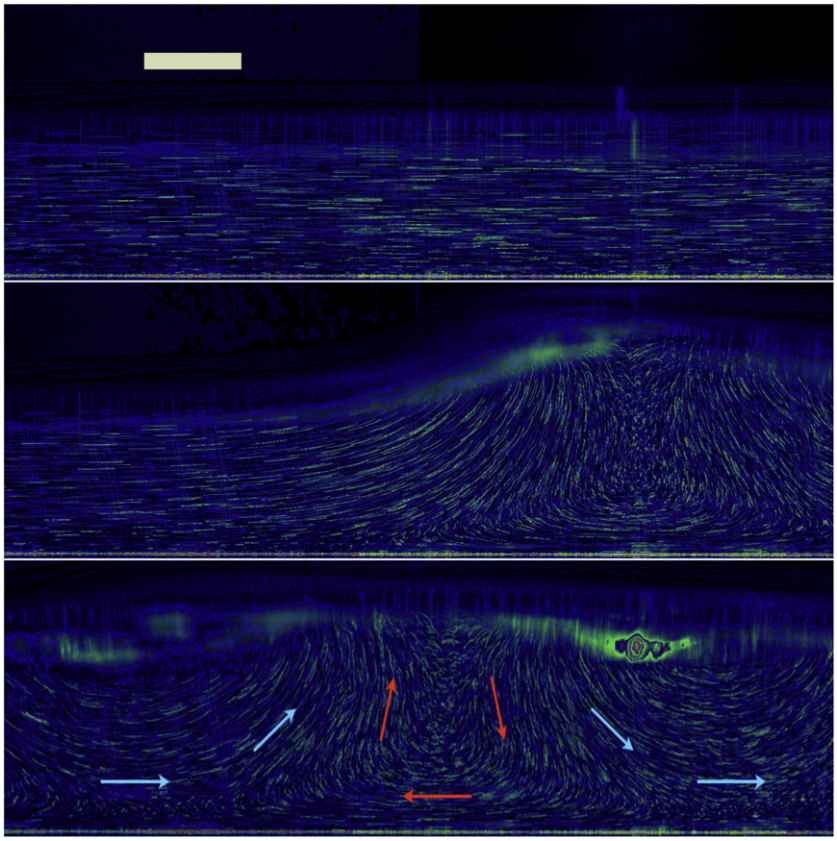

Fig. 5. Flow visualizations in false colors with tracers and a long exposure time (32 ms) to sketch the fluid streamlines (the bore propagates to the left). Top: at an arbitrary time when the water level decreases in an ebb-like way ($t = 0$ s); the scale corresponds to 20 mm. Middle: at $t = 1/3$ s when the leading front of the mini bore arrives in a flow-like way. Bottom: at $t = 0.4$ s under the first whelp ($h_0 = 25$ mm and $q_0 = 0.0215$ m^2/s).

will focus on detailed measurements of this behavior. Similar conclusions were reached by Bonneton et al. [4,7] where they discuss the influence of the so-called non-linear parameter which is essentially the local tidal range divided by the river water depth just before the bore. Unfortunately, as the theory of the tidal bore is not sufficiently developed, the reader will not find a comparison between our new procedure and the usual one. Indeed, no theoretical similitude rule allows us (for the moment) to design experiments that can be re-scaled and compared. As discussed in our recent paper where we study the flow below a bore generated by a fast-closing gate for several bottom boundary conditions, the emblematic dimensionless Froude number (which compare the effects of inertia and gravity) is unable to classify by itself the different types of bores observed and which are characterized by separate underwater conditions for the same Froude number [26]. Hence, it is currently impossible to correlate the experiments to real observations in the field. We hope that a theoretical group will find the similitude rules in order to allow comparisons between field, numerical and experimental studies: in particular, in the derivation of the Froude number scaling, one makes the hypothesis of hydrostaticity which is obviously wrong; one neglects also the friction. In their recent work, Bonneton et al. discussed the similitude rules for the propagation of a tidal bore in funnel-shaped estuaries for constant depth and an exponential decreasing width [7]: they take also into account the friction with a peculiar model. It remains to make the link with laboratory experiments whose channels have usually rectangular cross section which are constant. Moreover, the friction used in the equations of tidal wave propagation should be related to the velocity profiles measured in the laboratory. Finally, the present method should facilitate the understanding of the sediment transport induced by the tidal bore when compared to recent field studies [27,28]. In the near future, time resolved Particle Images Velocimetry measurements will focus on the particles trajectories and velocity fields as discussed in our recent paper using the classical procedure of generation [26].

Acknowledgments

We would like to thank warmly R. Bellanger and P.-J. Faltot for their help in the course of experiments. D. Pai improved the quality of the paper. G.R. would like to thank the Poitiers University for funding the present research (Action Concertée Incitative 2013). The water channel was funded by the FEDER 35790-2012. We are thankful to the french National Research Agency (ANR) for funding this work (2010 project “MASCARET” 091102).

Appendix

In this appendix, we resume well-known results [1,24] in order to characterize the hydraulic regimes of our water channel leading to our new natural procedure for bore production.

The acoustic sensor measuring the water depth was placed arbitrarily at 1.5 m downstream from the convergent exit. For deep water conditions (namely deeper than $h_0 = 240$ mm in Fig. 6 top), the dynamical water depth is always a decreasing function of the flow rate in the range accessible to the pump (up to 0.172 m^2/s). This decrease of the water depth is similar to the one observed when a current flows over a solid obstacle on the bottom of a river in a sub-critical regime [24]. When diminishing the static water depth h_0 (taking $h_0 = 100$ mm for example in Fig. 6 top), the dynamical water depth first decreases as before but reaches

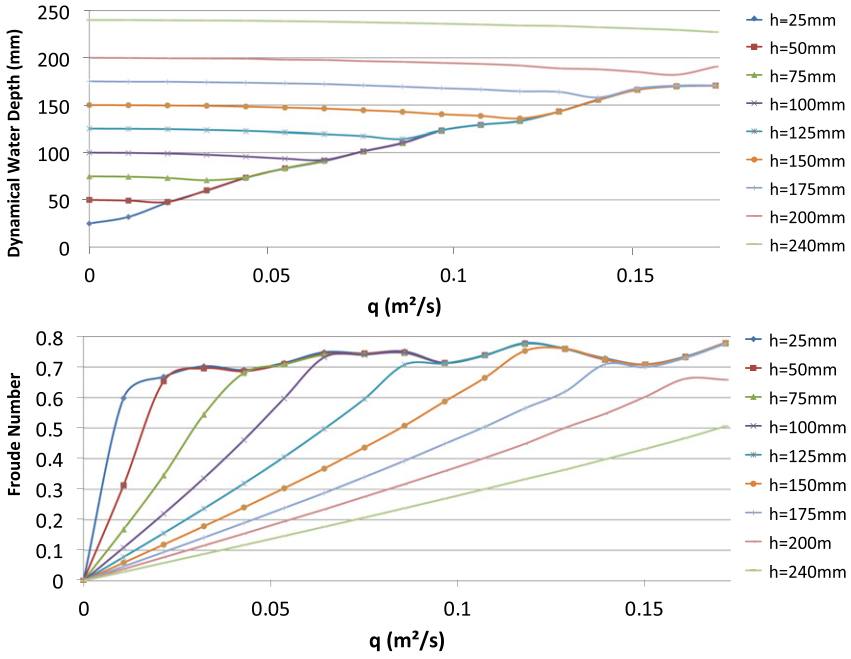

Fig. 6. Top: Dynamical water depth as a function of the pump flow rate q per unit width. Bottom: Froude number as a function of the flow rate q per unit width.

a minimum at a given flow rate ($q_{\min} = 0.065$ m^2/s for $h_0 = 100$ mm) and then increases regardless of the current intensity in the range accessible to the pump.

For the smaller static depths (less than $h_0 = 50$ mm in Fig. 6 top), the dynamical water depth keeps on rising for any flow rate. Whatever the initial static water depth, the dynamical water depth increases according to the same "universal" discharge curve. When converting the dynamical water depth in the dimensionless form of a Froude number (the ratio of the flow velocity q/h to the long wave velocity $\sqrt{gh}$ [24]) assuming a uniform velocity in the vertical direction, the threshold corresponds to a value close to 0.7 for the arbitrary position 1.5 m (see Fig. 6 bottom). There are oscillations around the maximum value of the Froude number (here 0.7 for 1.5 m) due to static undulations observed at the entrance of the hydraulic channel following the flow acceleration into the convergent part. These undulations are attenuated when moving along the water channel and are mostly damped at the channel end just before the exit chamber. When the Froude number at 1.5 m from the entrance is greater than 0.7, we observe in the exit chamber either a triangular-like shock pattern of the free surface or a spillway that no perturbation can penetrate indicating a supercritical flow with a transversally trapped bubble below the spillway for low flow rates and a spillway in ambient air for higher flow rates: as a well known fact in Hydraulics, the local Froude number reaches one at the exit of the channel.

During transients (for example, when one increases the flow rate q from 0.14 to 0.15 m^2/s at 150 mm water depth), the dynamic water depth increases with a typical exponential-like relaxation law before reaching a new higher value. On the contrary, when the Froude number at 1.5 m is less than 0.7, neither the shock triangle nor the spillway is observed at the very end of the channel in the entrance of the exit chamber, and surface perturbations can propagate upstream to the convergent chamber. Indeed, during transients (for example when one increase the flow rate q from 0.03 to 0.04 for m^2/s at 100 mm water depth), the dynamic water depth decreases in an oscillating fashion with an exponential-like envelope. These oscillations are due to the channel modes such that very long waves are reflected at both extremities of the channel on the vertical wall of the exit chamber and on the honeycomb of the convergent entrance. For small flow rates and high water depths, it is necessary to wait for the disappearance of the oscillations before performing measurements of the dynamical water depth.

To resume and as already well understood, the local Froude number in the channel exit chamber reaches one at the position of the spillway and/or of the triangular shock if the oscillations disappear, namely when the flow becomes supercritical. In the latter case, it is easy to understand that the dynamical water depth keeps increasing with the flow rate, similarly to the flow over an obstacle in the supercritical regime. For the smaller static water depths, we have seen that the dynamical water depth is an increasing function of the flow rate and no perturbations can propagate upstream since a blocking line is present at the very end of the channel in the shock and/or spillway region.

References

[1] H. Chanson, Tidal Bores, Aegir, Eagre, Mascaret, Pororoca: Theory and Observations, World Scientific, Singapore, 2011.
[2] S. David Graber, Perspective on the tidal bore: Background and initiation, in: Proceedings of the ASME 2012 Fluids Engineering Summer Meeting FEDSM2012, July 8–12, 2012, Rio Grande, Puerto Rico, USA, Paper No. FEDSM2012-72112, 2012, pp. 211–221.
[3] S. David Graber, Perspective on the tidal bore: Channel taper, friction, building, maximum height, variation, dissipation, in: Proceedings of the ASME 2012 Fluids Engineering Summer Meeting FEDSM2012, July 8–12, 2012, Rio Grande, Puerto Rico, USA, Paper No. FEDSM2012-72114, 2012, pp. 223–233.
[4] N. Bonneton, P. Bonneton, J.-P. Parisot, A. Sottolichio, G. Detandt, Tidal bore and Mascaret—example of Garonne and Seine Rivers, C. R. Géosci. 344 (10) (2012) 508–515.
[5] E.N. Dolgopolova, The conditions for tidal bore formation and its effect on the transport of saline water at river mouths, Water Resour. 40 (1) (2013) 16–30.
[6] H. Chanson, Tidal bore research: field works, physical modeling, CFD & more, in: 35th IAHR World Congress, Chengdu, China, Proceedings of the 35th IAHR World Congress, 8–13 September, 2013.
[7] P. Bonneton, N. Bonneton, J.-P. Parisot, B. Castelle, Tidal bore dynamics in funnel-shaped estuary, J. Geophys. Res.: Oceans 120 (2015).
[8] R. Ethersey, On the bore, or rushing tide, in the gulf of cambay, and at the entrances of the mahi and Sabarmati rivers, J. R. Geogr. Soc. Lond. 8 (1838) 196–202.
[9] H. Partiot, Mémoire sur le Mascaret, Ann. Ponts Chaussées 1 (Ser. 4, T1) (1861) 17–48.
[10] M. Vauthier, Sur le Mascaret de la Seine Observé le 20 Septembre 1880, in: La Seine maritime et son estuaire, in: Encyclopédie des Travaux Maritimes, 1885.
[11] A. Dormoy, Notions sur le Mascaret de la Seine (Pour servir à l'étude du même phénomène dans les fleuves à grandes marées), Revue maritime et coloniale—Ministère de la marine et des colonies, 1892, pp. 560–580.
[12] A. Brownlie, The solution of the problem of the tidal bore, Bull. Am. Geogr. Soc. 33 (4) (1901) 318–324.

[13] H.H. Champion, R.H. Corkan, The bore in the trent, Proc. R. Soc. Lond. Ser. A Math. Phys. Sci. 154 (881) (1936) 158–181.
[14] R.S. Shri, M.A. Chugh, Tides in Hooghly river, Int. Assoc. Sci. Hydrol. Bull. 6 (2) (1961) 10–26.
[15] N. Mazumder, P. Chatterjee, S. Basak, Generation of bore, J. Waterw. Port Coastal Ocean Eng. 110 (2) (1984) 159–170.
[16] G. Bidone, Expériences sur la propagation du remous, Imprimerie royale, Turin, 1825.
[17] V.I. Bukreev, Undular bore in the counterflow, Dokl. Phys. 45 (8) (2000) 422–424.
[18] H. Chanson, K.K. Tan, Turbulent mixing of particles under tidal bores: an experimental analysis, J. Hydraul. Res. IAHR 48 (5) (2010) 641–649.
[19] J. Huang, C. Pan, C. Kuang, Experimental hydrodynamic study of the Qiantang river tidal bore, J. Hydrodyn. 25 (3) (2013) 481–490.
[20] H. Darcy, H. Bazin, Recherches Hydrauliques—entreprises par M. Henry Darcy continues par M. Henry Bazin. Mémoire en deux parties (Recherches expérimentales sur l'écoulement de l'eau dans les canaux découverts; Recherches expérimentales relatives au remous et la propagation des ondes), Dunod, Paris, Imprimerie impériale, 1865.
[21] H. Favre, Ondes de translation dans les canaux découverts, Dunod, 1935.
[22] H.-H. Pruser, W. Zielke, Undular bores (favre waves) in open channels theory and numerical simulation, J. Hydraul. Res. 32 (3) (1994) 337–354.
[23] A. Treske, Undular bores (favre-waves) in open channels—Experimental studies, J. Hydraul. Res. 32 (3) (1994) 355–370.
[24] M. Hanif Chaudry, Open Channel Flow, Springer, 2008.
[25] M. Cross, P. Hohenberg, Pattern formation outside of equilibrium, Rev. Modern Phys. 65 (1993) 851.
[26] L. David, L. Chatellier, D. Calluaud, Y.J. Jeon, G. Rousseaux, L. Thomas, TR-PIV measurements in open channel flow for the analysis of undular tidal bores, in: Proceedings of the 17th International Symposium on Applications of Laser Techniques to Fluid Mechanics Lisbon, Portugal, 07–10 July, 2014. http://ltces.dem.ist.utl.pt/lxlaser/lxlaser2014/finalworks2014/papers/02.12_5_251paper.pdf.
[27] L. Furgerot, D. Mouaz, B. Tessier, L. Perez, Suspended sediment concentration in relation to the passage of a tidal bore (See river estuary, Mont Saint Michel bay, NW France), in: Proceedings of the 7th International Conference on Coastal Dynamics, Arcachon, France, 2013.
[28] C.E. Keevil, H. Chanson, D. Reungoat, Fluid flow and sediment entrainment in the garonne river bore and tidal bore collision, Earth Surf. Process. Landf. XX (2015).